European Journal of Medicinal Chemistry 214 (2021) 113210

Contents lists available at ScienceDirect

European Journal of Medicinal Chemistry

journal homepage: http://www.elsevier.com/locate/ejmech

Targeting the transmembrane domain 5 of latent membrane protein 1 using small molecule modulators

Bo Zhang [a, b], Yibo Wang [a], Cong Lin [a], Hongyuan Li [a], Xiaojie Wang [a], Yinghua Peng [c], Konstatin S. Mineev [d, e], Andrew J. Wilson [f, g], Hongshuang Wang [a, **], Xiaohui Wang [a, b, *]

[a] Laboratory of Chemical Biology, Changchun Institute of Applied Chemistry, Chinese Academy of Sciences, Changchun, Jilin, 130022, China
[b] Department of Applied Chemistry and Engineering, University of Science and Technology of China, Hefei, Anhui, 230026, China
[c] State Key Laboratory for Molecular Biology of Special Wild Economic Animals, Institute of Special Animal and Plant Sciences, Chinese Academy of Agricultural Sciences, Changchun, Jilin, 130112, China
[d] Shemyakin–Ovchinnikov Institute of Bioorganic Chemistry, Russian Academy of Sciences, Moscow, 117997, Russia
[e] Department of Biological and Medicinal Physics, Moscow Institute of Physics and Technology, Dolgoprudny, 141701, Russia
[f] School of Chemistry, University of Leeds, Woodhouse Lane, Leeds, LS2 9JT, UK
[g] Astbury Centre for Structural Molecular Biology, University of Leeds, Woodhouse Lane, Leeds, LS2 9JT, UK

ARTICLE INFO

Article history:
Received 21 November 2020
Received in revised form
14 January 2021
Accepted 14 January 2021
Available online 27 January 2021

Keywords:
Protein-protein interactions
Pentamidine analogues
Latent membrane protein 1
The fifth transmembrane domain (TMD-5)
Epstein-barr virus
Small molecule modulators

ABSTRACT

Protein-protein interactions (PPIs) play a critical role in living cells and represent promising targets for the drug discovery and life sciences communities. However, lateral transmembrane PPIs are difficult targets for small-molecule inhibitor development given less structural information is known and fewer ligand discovery methods have been explored compared to soluble proteins. In this study, the interactions of the transmembrane domain 5 (TMD-5) of latent membrane protein 1 (LMP-1) of Epstein-Barr virus (EBV) were disrupted by pentamidine derivatives to curb the committed step of EBV infection. A pentamidine derivative **2** with a 7-atom di-amide linker had the best activity whilst switching the amide regiochemistry in the linker influenced membrane permeability and abolished anti TMD-5 activity. Molecular dynamics simulations were performed to understand the interaction between pentamidine derivatives and TMD-5, and to rationalise the observed structure-activity relationships. This study explicitly demonstrated that the interaction of small molecule with lipid should be considered alongside interaction with the protein target when designing small molecules targeting the PPIs of TMDs. In all, this study provides proof of concept for the rational design of small molecules targeting transmembrane PPIs.

1. Introduction

Protein-protein interactions (PPIs) are fundamental for living cells [1,2]. However, until recently they were considered undruggable given that PPI interfaces are typically large and flatter than those usually targeted by small molecules [3]. Lateral transmembrane PPIs are even more difficult to probe because less structural information is known and fewer ligand discovery methods have been applied to the identification of inhibitors when compared to soluble proteins [4]. Despite the hydrophobic nature of the transmembrane helix, the presence of charged residues is believed to be important for membrane protein functions [5–8]. For instance, with assistance of a charged aspartic acid (D150) in its transmembrane domain 5 (TMD-5) [9], the oncogenic latent membrane protein 1 (LMP-1) of Epstein-Barr virus (EBV) can form homo-oligomeric complexes on lipid rafts to active downstream signaling, leading to cell transformation [10–13]. As the first human cancer virus to be discovered, it is highly infectious and about 90% of the world's population is infected [14]. Studies have shown that EBV infection is highly correlated with multiple malignancies, including Burkitt's lymphoma, Hodgkin's lymphoma, stomach cancer, nasopharyngeal carcinoma, etc. [15–17] Unfortunately, LMP-1 function is independent of ligand binding and it effectively serves as a constitutively active receptor following oligomerization

* Corresponding author. Laboratory of Chemical Biology, Changchun Institute of Applied Chemistry, Chinese Academy of Sciences, Changchun, Jilin, 130022, China.
** Corresponding author.
E-mail addresses: hongshuang.wang@ciac.ac.cn (H. Wang), xiaohui.wang@ciac.ac.cn (X. Wang).

https://doi.org/10.1016/j.ejmech.2021.113210
0223-5234/

[18]. Therefore, the lateral transmembrane PPIs between monomers represent one of the limited current targets for drug discovery against EBV. Recent studies showed that TMD-5 itself can also form an oligomer [9,19], rendering it an ideal model for small molecule screening and development targeting LMP-1 to curb the committed step of EBV infection [20–22]. Pentamidine, which is a clinical antifungal medication, has been shown to disrupt the oligomerization of LMP-1 (Fig. 1) [20,21]. However, its inhibition efficiency is moderate and its molecular mechanism of action is not well understood. Herein pentamidine analogues **1**–**5** with linkers of different lengths, varieties and orientations were designed and their anti TMD-5 activities were tested. A pentamidine derivative with a 7-atom di-amide linker, **2**, had the best activity. Interestingly, switching the regiochemistry of the amides in the linker to give a pentanediamide derivative abolished anti TMD-5 activity. Further molecular dynamics simulations were performed to understand the interaction between the small molecules **1**–**5** and TMD-5, and to rationalise the observed structure-activity relationships (SAR).

2. Results and discussion

The chemical structure of pentamidine (Fig. 1) is symmetrical and contains two benzamidine motifs coupled by a bis(oxy)-pentane linker. Previous limited SAR studies showed that the positively charged benzamidine group is critical for anti TMD-5 activity [20,21]. However, how the linker affects its anti TMD-5 activity is not clear. Herein SAR analyses on the linker connecting two benzamidine groups in pentamidine was explored. Considering that only hydrogen bond acceptors (oxygens) exist in the linker of pentamidine, amide or secondary amine groups (both hydrogen bond acceptors and donors) were incorporated into pentamidine analogues to enhance protein-ligand interactions.

An *E. coli* FHK-12 cell-based ToxR assay was developed to study the association of the transmembrane helix in a biological membrane [23,24]. The chimeric TMD-5 was expressed with maltose binding protein for localization on the membrane and transcription factor ToxR to provide a reporter for changes in oligomerization. As shown in Fig. 2 and Table 1, pentamidine derivative **2**, which was constructed by replacing the bis(oxy)-pentane linker of pentamidine with pentanediamide and has the same number of linker atoms as pentamidine, inhibited ToxR activity in a concentration-dependent manner with an IC_{50} of 0.6 ± 0.3 μM, which is 15-fold higher than pentamidine (9.1 ± 0.6 μM) [21], suggesting it could disrupt the oligomerization of TMD-5. By changing the linker length by one-atom with respect to **2**, **1** was formed by linking two benzamidine motifs with butanediamide and **3** was designed by linking the benzamidine motifs with hexanediamide. Compared to **2**, **1** (IC_{50} = 111.5 ± 15.0 μM) and **3** (IC_{50} = 42.0 ± 14.8 μM) showed much weaker anti TMD-5 potencies, which indicates that the length of the linker is critical and a linker of 7-atoms in length is optimal. However, switching the

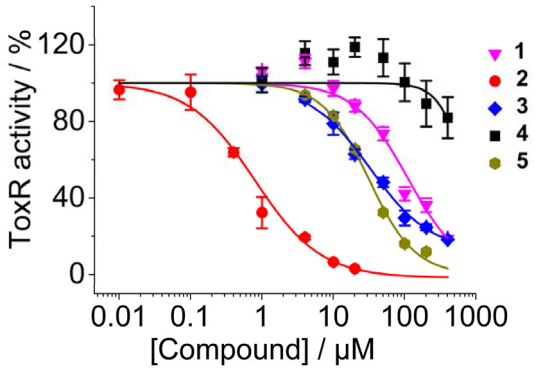

Fig. 2. Concentration-dependent inhibition curves of pentamidine analogues on TMD-5 oligomerization was measured by chimeric TMD-5 ToxR assay.

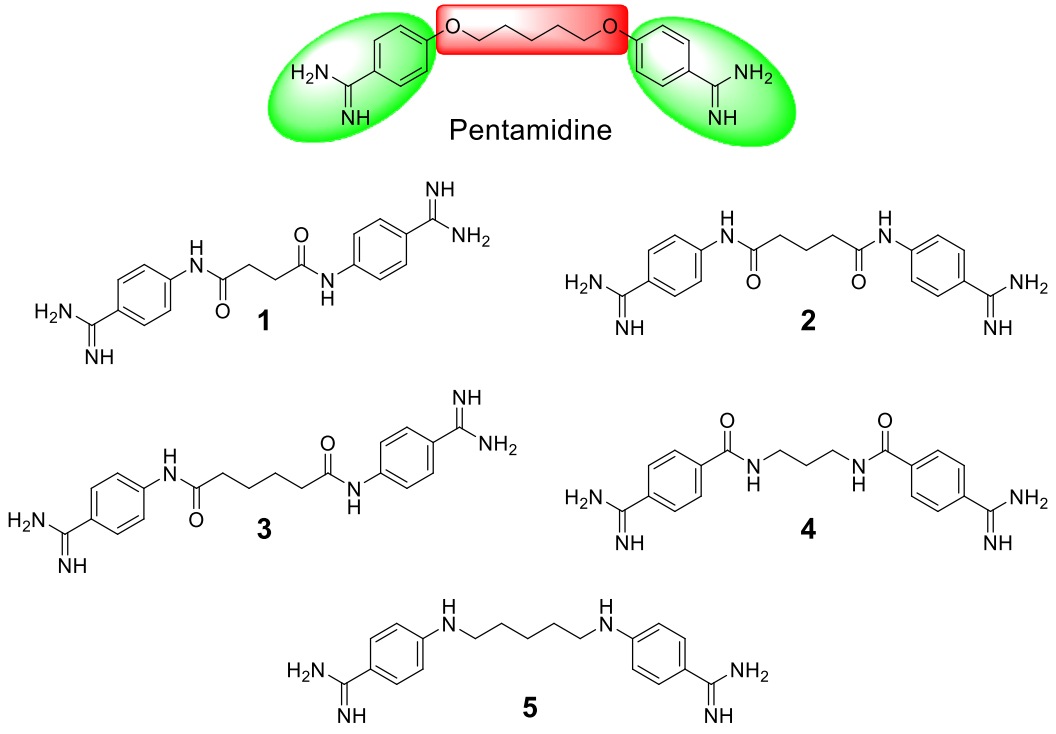

Fig. 1. Chemical structures of pentamidine and its derivatives **1**–**5**. The linker is highlighted in red in pentamidine.

Table 1
IC_{50} for ToxR assay, cell viability and TMD-5 binding affinity (K_d) of pentamidine analogues.

Compound	IC_{50} of ToxR (μM)	FHK 12 cell viability (μM)	K_d (μM)
1	111.5 ± 15.0	>200	13.5 ± 3.3
2	0.6 ± 0.3	56.4 ± 2.1	2.6 ± 0.4
3	42.0 ± 14.8	>200	8.9 ± 2.3
4	>200	>200	*n.d*
5	31.2 ± 1.4	>200	7.3 ± 1.8

n.d., not determined because the binding affinity was too weak to fit; All experiments were performed at least three times independently, and data are given as the mean ± SD.

regiochemistry of the amide from **2** to give **4** resulted in the abolition of anti TMD-5 activity (IC_{50} > 200 μM), which revealed a critical importance of amide orientation on inhibitory potency. Changing the linker from an ether group (pentamidine) or amide group (**2**) to an amino group (**5**), the anti TMD-5 activity also diminished (IC_{50} = 31.2 ± 1.4 μM). It should be noted that no derivative showed significant cell proliferation inhibition (Table 1 for cell viability). Together, the results showed the linker composition, length and the functional group orientation profoundly influence pentamidine derivative's anti TMD-5 activity.

To further confirm the interaction between pentamidine derivatives and the chimeric TMD-5 system happened in the membrane domain, a direct TMD-5 biophysical binding experiment in the membrane environment was performed [9]. Tryptophan (Trp) emission fluorescence intensity of TMD-5 was recorded upon titration with pentamidine derivatives; this led to quenching of the TMD-5 intrinsic fluorescence (Fig. 3). The dissociation constants are summarized in Table 1. A dissociation constant of 2.6 ± 0.4 μM was determined for **2**. Compared to **2**, **1** (K_d = 13.5 ± 3.3 μM) and **3** (K_d = 8.9 ± 2.3 μM) had weaker binding affinity to TMD-5, which is consistent with the TMD-5 ToxR functional assays and confirmed the optimal linker of 7-atoms for pentamidine analogues. Interestingly, the binding affinity of **4**, which was designed by reversing the orientation of the amides in the linker of **2**, was too weak to fit. Finally, the TMD-5 binding affinity of **5** was 7.3 ± 1.8 μM, again weaker than that of **2**. Collectively, the TMD-5 biophysical binding data were consistent with the TMD-5 ToxR activity data and confirmed the linker profoundly influences the anti-TMD-5 activity of pentamidine derivatives.

Molecular dynamics (MD) simulations were employed to understand how pentamidine derivatives interact with TMD-5 and to rationalise the observed SAR. The root-mean-square deviation (RMSD) of TMD-5 over 50 ns was analyzed across the series of pentamidine analogues (Fig. 4). The RMSD values of TMD-5 in the protein-ligand complexes showed that all TMD5s can reach a stable state in 50 ns.

Binding mode analysis showed that all compounds exhibited similar interaction patterns with TMD-5: one amidine group interacted with the charged D150 of TMD-5 to sterically encumber oligomer formation whilst the other amidine group reached out to the polar head group of the membrane lipids (Fig. 5). **1**, **3** and **5** caused bending of TMD-5 in the membrane (the bending angles of TMD-5 are shown in Fig. S1), which would incur an energy penalty and therefore reduce the TMD-5 binding affinity and anti-TMD activity. In contrast, **2** and **4**, had much less influence on conformational changes of TMD-5 than the other compounds, which indicated that a lower energy penalty was required to bend TMD-5 when **2** or **4** binds to TMD-5.

Interactions of the linker nitrogen with the lipid head groups, which appear to be a key driving force for bending of TMD-5 in the membrane, were further investigated. Compared to other pentamidine derivatives, **2** and **4** showed formation of fewer H-bonds between linker nitrogen and lipid head groups (Fig. 6, white columns). Meanwhile, **4** is the only analogue with an electron withdrawing group para to the amidine, decreasing the ability of forming hydrogen bonds of amidines. As shown in Fig. 6 (grey columns), amidines of **4** formed the fewest hydrogen bonds with TMD-5 among all pentamidine analogues. These provide an explanation as to why they did not substantially bend the TMD-5 helix. Together, these MD simulations in the membrane milieu indicate that **2** and **4** should have potent TMD-5 binding affinity and anti-TMD activity. However, experimental evidence indicated that **2** was a potent TMD-5 disruptor while **4** had no apparent anti-TMD-5 activity.

It should be noted that during the above MD simulations the small molecules were first directly docked into TMD-5 in the membrane milieu. Considering that pentamidine derivatives first permeate into the membrane and then interact with TMD-5, it was therefore speculated that **4** might have poor membrane permeability. In order to test this hypothesis, the free energy changes for **2** and **4** crossing the membrane were calculated. As shown in Fig. 7A, **2** overcame an energy barrier of 1.5 kcal/mol to enter the membrane and stayed in the middle of membrane with a free energy change of −6.8 kcal/mol; **4** had to overcome an energy barrier with ~3.0 kcal/mol to permeate into the membrane and had a free energy minimum of −4.9 kcal/mol. Compared to **2**, the parameters

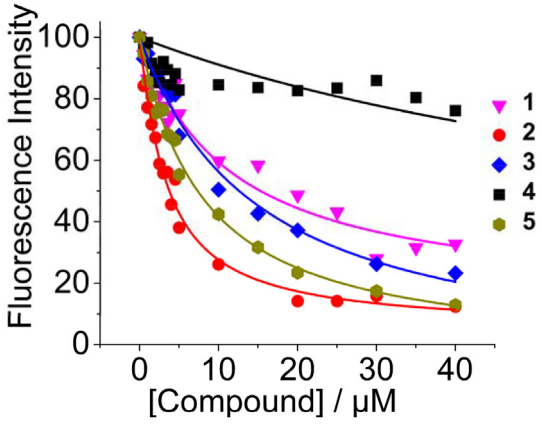

Fig. 3. Representative titration curves of TMD-5 with pentamidine analogues. 290 nm was used as the excitation wavelength for intrinsic Trp protein fluorescence; emission fluorescence at 337 nm was plotted against the pentamidine analogue concentration.

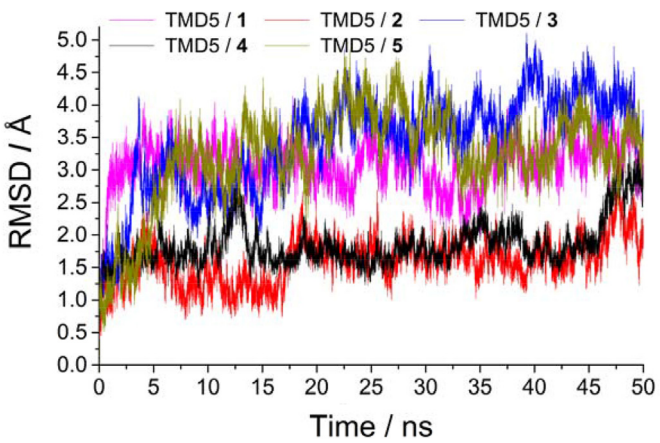

Fig. 4. Time evolution curves of RMSD of TMD-5 helix backbone during molecular dynamics simulations of TMD-5/pentamidine analogue complexes.

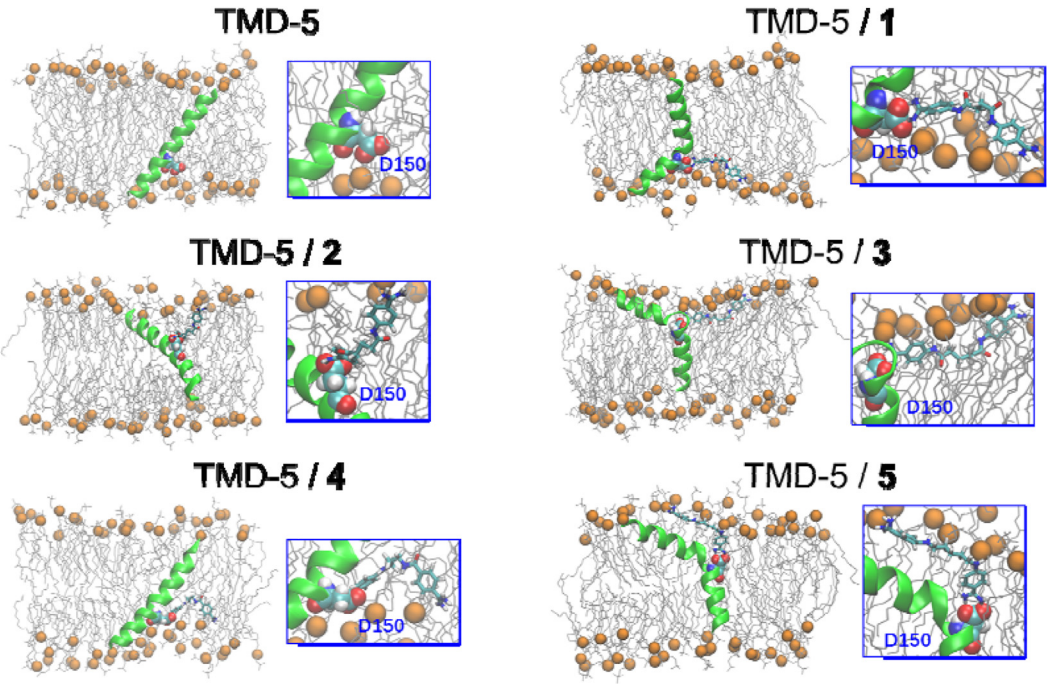

Fig. 5. Conformations of TMD-5 with pentamidine analogues after equilibration. The grey lines represent the lipids and the orange spheres represent phosphorus atoms in the lipids. TMD-5 is shown as a green ribbon. The key residue D150 is shown with spheres and the cyan sticks correspond to the compounds.

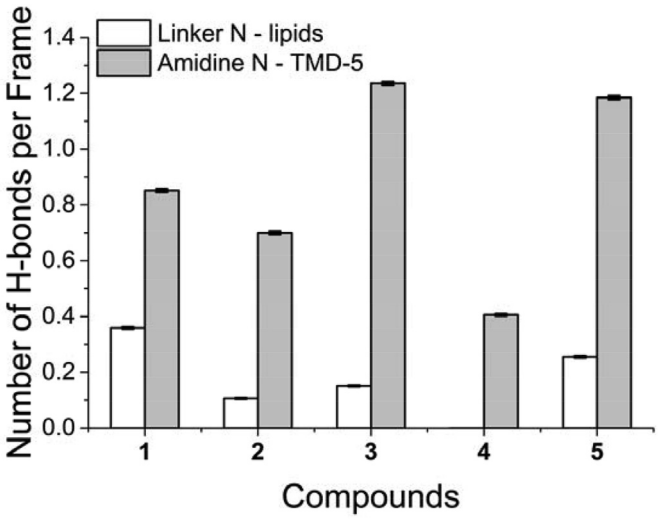

Fig. 6. Number of H-bonds per frame (total number of H-bonds/number of frames) formed between nitrogen in the linker and lipids (white columns) and between nitrogen in amidines and TMD-5 (grey columns).

governing partition of **4** into the membrane milieu were kinetically and thermodynamically less favorable. To validate the calculation results about pentamidine derivatives **2** and **4** crossing cell membranes, the MDCK transport experiments were performed. The apparent permeability coefficient (P_{app}) of compounds **2** and **4** are shown in Fig. 7B. An apparent permeability coefficient (P_{app}) of $4.28 \times 10^{-6} \pm 1.24 \times 10^{-7}$ cm/s was determined for **2**. Compared to **2**, **4** ($P_{app} = 1.07 \times 10^{-6} \pm 1.03 \times 10^{-7}$ cm/s) had much weaker membrane penetration ability, which is consistent with the above free energy calculations. Therefore, **4**, generated by switching the position of the carbonyl group and amino group relative to the linker in **2**, showed weak ability to bind and disrupt TMD-5 oligomerization which is most likely due to its poor membrane permeability. In contrast, **2**, which had better membrane permeability, interacted with TMD-5 without apparent bending of the TMD-5 helix, favoring TMD-5 binding and TMD-5 oligomerization disruptor activity.

The free energy profiles for **2** binding to TMD-5 are shown in Fig. 8. In the PMF profiles, compound **2** reached a global minimum at z = 5.5 Å with −4.6 kcal/mol. However, the minimum for **4** is at z = −0.5 Å with −3.6 kcal/mol. The conformations and locations with lowest free energy of compounds **2** and **4** interacting with TMD-5 are consistent with the equilibrium simulation results (see Fig. 5). Significantly, the presence of TMD-5 decreased the energy barrier for compound permeation into the membrane. However, the barrier for permeation of **4** is still slightly higher than **2** whilst binding of **4** is less favorable than that of **2** based on the free energies. Considering the broader permeation barrier for **4**, it may be kinetically unfavourable for **4** to enter the membrane even in the presence of TMD-5.

3. Conclusions

We designed pentamidine analogues to disrupt the oligomerization of TMD-5 by targeting D150. **2** with a linker length of 7 atoms had the best activity whilst switching the amide regiochemistry in the linker influenced membrane permeability and abrogated anti TMD-5 activity. Further examination of the effects of pentamidine derivatives on the oligomerization and function of full length of LMP-1 of EBV is worthy of investigation. In contrast to traditional drug discovery, targeting the PPIs of TMD is a multibody problem; the interaction of small molecule with lipid should be considered alongside small molecule interactions with target proteins, and target protein-lipid interactions. The permeability of the small molecule, which may be influenced by the structural orientation of its functional groups, is critical because local lipophilicity is likely to influence conformation, stability, and

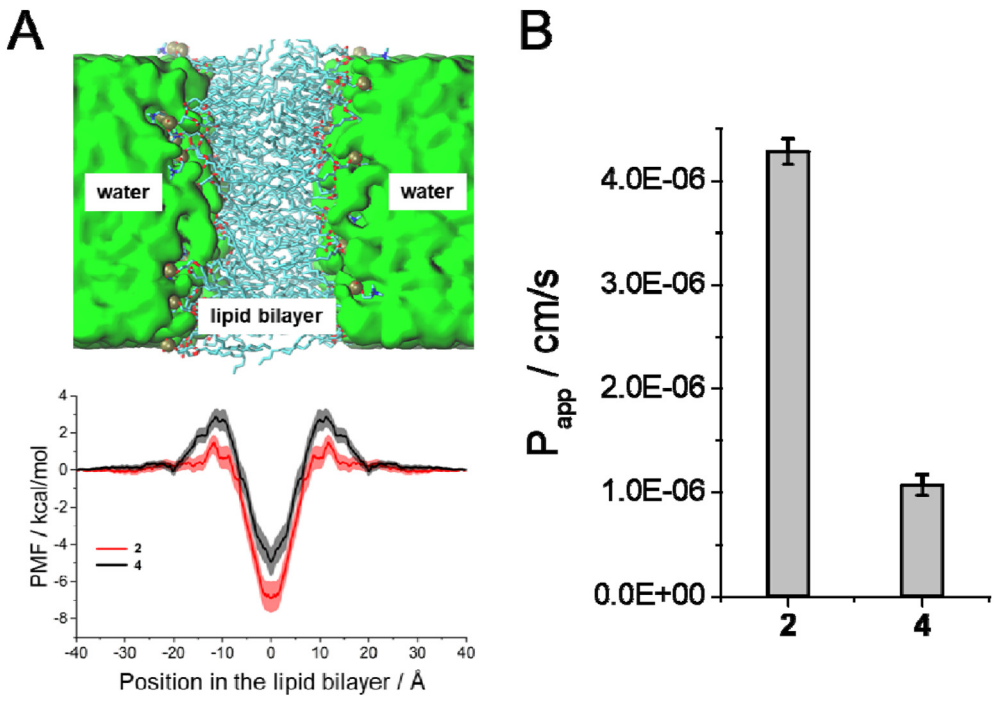

Fig. 7. (A) The free energy profiles (PMFs) along the permeation route of pentamidine analogues into a model bilayer; (B) The apparent permeability coefficient (P_{app}) of pentamidine analogues **2** and **4** was measured by MDCK transport experiments.

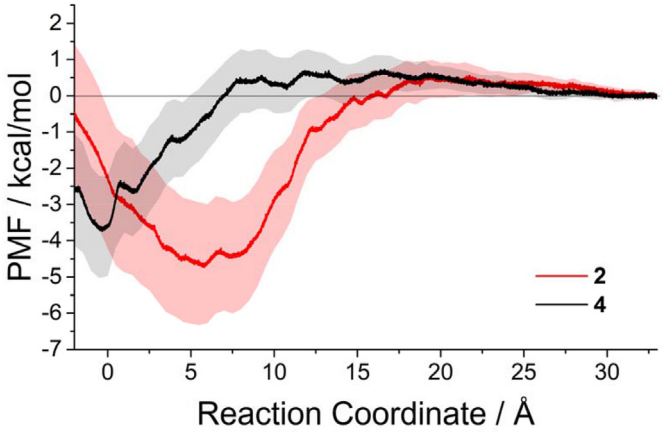

Fig. 8. The binding free energy profiles of compounds **2** and **4** interacting with TMD-5. The reaction coordinate was defined as the distance along the z axis between the center of mass of non-hydrogen atoms of the compound and the carbon atom of the carboxyl group of D150 (see Fig. S2).

oligomerization in the transmembrane domain. In all, this study provides proof of concept for the rational design of small molecules targeting transmembrane PPIs.

4. Materials and method

4.1. ToxR assay

ToxR assay was performed and validated as described previously (Scheme 1) [20,21]. Briefly, ToxR7-TMD-5 plasmid (200 ng) was transformed into 200 μL FHK12 competent cells with heat shock at 42 °C for 90 s and incubated on ice for 2 min, followed by addition of 800 μL SOC media and incubation with shaking at 37 °C for 1 h. 50 μL of the transformation mixture was used to inoculate 5 mL LB + arabinose (0.0025%) and chloramphenicol (30 μg/mL) with different concentrations of testing compound. Five replica Cultures were incubated with shaking at 37 °C for 20 h and β-galactosidase activity was measured using a SYNERGY H1 Micro-plate Reader (BioTek Instruments, Carlsbad, CA, USA). Briefly, 5 μL of culture was transferred to the wells of a Costar 3596 polystyrene 96-well plate (Corning, NY, USA) containing 100 μL Z buffer/chloroform (1% β-mercaptoethanol, 10% chloroform, 89% A buffer: 1 M sodium phosphate, 10 mM KCl, 1 mM $MgSO_4$ and pH 7.0). Cells were lysed by addition of 50 μL Z buffer/SDS (1.6% w/v sodium dodecyl sulfate in Z buffer) and shaking at 28 °C for 10 min. 50 μL Z buffer/*o*-Nitrophenyl-β-galactoside (ONPG, 0.4% w/v in Z buffer) was added and β-galactosidase activity was measured by monitoring the reaction at 405 nm for a period of 20 min at 28 °C. The effect of testing compound on FHK12 *E. coli*. proliferation was also investigated by measuring the OD at 600 nm (Table 1).

4.2. Peptide synthesis

TMD-5 peptide (KKKK-WQLLAFFLAFFLDLILLIIALYL-KKKK) was synthesized and purified by a CRO company (GL Biochem, Shanghai, China). The identity and purity of this peptide was confirmed by MALDI and HPLC (>98%) (Fig. S8 and S9). The concentration of TMD-5 was determined by absorbance at 280 nm using the extinction coefficient of 6990 $M^{-1}cm^{-1}$.

4.3. Biophysical binding titration

The intrinsic Trp fluorescence of TMD-5 was used to investigate the interaction of TMD-5 with pentamidine analogues. Fluorescence measurements were performed on a Cary Eclipse spectrofluorimeter (Agilent Technologies, Santa Clara, CA, USA). All measurements were carried out under room temperature in a 2 × 10 mm quartz cell (Starna Cells, Atascadero, CA, USA). 290 nm was chosen as the excitation wavelength of Trp fluorescence and

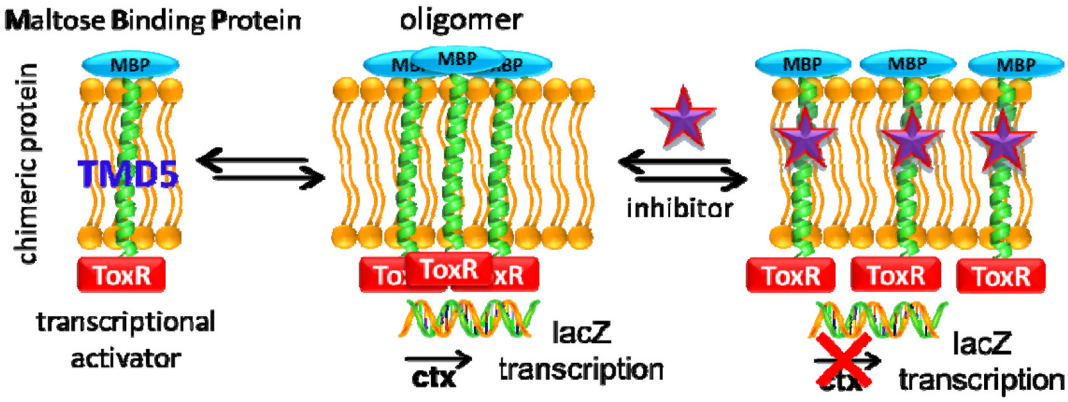

Scheme 1. ToxR assay. TMD-5 can self-associate in an *E. coli* Membrane to activate the transcriptional activator ToxR, promoting binding to the *ctx* promoter and initiating *lacZ* transcription. It will further regulate the production of β-galactosidase. A colorimetric readout is obtained by addition of ONPG to lysed cells.

emission at 310–450 nm was measured. Appropriate controls were subtracted from spectra obtained on the samples. 1 μM TMD-5 in 50 mM HEPES (pH = 7.4) buffer contained 150 μM C14 betaine (3-(*N*,*N*-dimethyl- myristylammonio)propanesulfonate) micelle was titrated with different concentrations of testing compound. The fluorescence intensity at 337 nm was plotted against compound concentration. The raw data was fitted by non-linear least square method using the equation:

$$F = 0.5 \times (2 \times F_0\text{-}F_{PL} \times (K_D+[L_T]+[P_T]\text{-}((K_D+[L_T]+[P_T])^2\text{-}4 \times [L_T] \times [P_T])^{0.5}))$$

where *F*, the observed fluorescence; F_0, initial fluorescence of protein in the absence of ligand; F_{PL}, adjustable parameter for protein-ligand complex molar fluorescence; K_D, dissociation constant; $[L_T]$, total concentration of the ligand; $[P_T]$, total protein concentration.

4.4. Docking

The structure for the TMD-5 was built as described previously [22]. The state of D150 was set to be charged and the compounds were prepared by Maestro [25]. The charge state of compounds were generated at pH = 7.0 ± 2.0 (all compounds are protonated with the charge of +2). AutoDock Vina 1.1.2 [26] was applied with default setting options to dock and score the compounds. The best scored conformations were used for molecular dynamics simulations.

4.5. Molecular simulations

The TMD-5 helix and compound were embedded in a 1,2-dimyristoyl-sn-glycero-3-phosphocholine (DMPC) bilayer and solvated with TIP3P water molecules in a 60 × 60 × 120 $Å^3$ box via the CHARMM-GUI membrane builder protocol [27]. 150 mM KCl was added to neutralize the system and mimic the physiological concentration. The protein, lipids, and ions were described by the CHARMM36 force field [28,29] and compounds **1**, **2**, **3**, and **4** were parameterized by the CGenFF program [30]. Considering that the penalties of compound **5** was too high, it was re-parameterized with GAAMP program [31]. All MD simulations were performed by the NAMD2.12 program package [32].

The models with ~40,000 atoms were simulated under the NPaT ensemble with a pressure of 1 atm at 310.15 K. The Nosé-Hoover Langevin piston method [33,34] was applied for the pressure control and the Langevin thermostat for the temperature coupling. The particle mesh Ewald (PME) algorithm was employed to treat long-range electrostatic interactions [35]. Non-bonded interactions were switched off at 10–12 Å and periodic boundary conditions were applied in all directions. The timestep was set as 2 fs and each system was run for 50 ns. Only the last 30 ns were used for hydrogen bond analysis.

The compound permeation simulations were set with the same conditions. To explore the free energy changes when compounds permeate into the lipid bilayer, umbrella sampling simulations were performed. A harmonic biasing potential with a force constant of 10 kcal/(mol·Å) along the perpendicular direction of lipid bilayer was applied on the center of mass (COM) of non-hydrogen atoms of compounds. The sampling windows were spaced every 0.5 Å from −40 to 40 Å resulting in 161 windows. Each window was run for 3 ns as only the last 2 ns was used for analysis. The free energy profiles were rebuilt with the Weighted Histogram Analysis Method (WHAM) and the tolerance was set to 10^{-6} [36,37]. The statistical uncertainties were estimated as described previously [38].

Free energy profiles of compounds binding to TMD-5 were also calculated by umbrella sampling methods. Same simulation conditions described above for compound permeation simulations were applied. The reaction coordination was defined as the distance along z axis between the COM of non-hydrogen atoms of compound and the carbon atom of carboxyl group of D150 (see Fig. S2). Each window was run for 11 ns as only the last 10 ns was used for analysis.

4.6. MDCK transport experiment

Dulbecco's Modified Eagle's Medium (DMEM) and Trypsin–EDTA were purchased from HyClone (Uath, USA). Penicillin, streptomycin and G418 (+10000 Units/mL penicilin, +10000 μg/mL streptomycin) were purchased from Grand Island (NY, USA). Foetal bovine serum (FBS) and Hank's Balanced Salt Solution (HBSS) were obtained from BI (Biological Industries Israel Beit Haemek LTD., CT, USA). Transwell™ plates of 12 wells (12 mm, pore size 0.4 μm) were purchased from Corning Costar (Cambridge, MA, USA).

4.6.1. Cell culture and evaluate the viability of cells

MDCK cells were cultured in DMEM, supplemented with 10% (v/v) FBS, 1% penicillin-streptomycin solution and 0.5 mL G418 solution (600 μ g/mL) at 37 °C in an incubator containing 5% CO_2.

The passage number of the cells was 20–35. Viability of cells was directly measured using MTT assay to evaluate the maximum nontoxic concentration to the cells (Fig. S3). For the MTT assay, MDCK cells were seeded onto a 96-well culture plate with a density

of 4000 cells/well and incubated at 37 °C for 24 h. Then the medium was replaced with 100 μM pentamidine analogues **2** and **4** with different concentrations, which diluted in DMEM containing 10% FBS. The control group was treated with the same amount solvent without drugs. Meanwhile, the wells without cells were used as blank control. After 4 h, the medium was replaced with 100 μL MTT at the concentration of 1 mg/mL to form formazan crystals. And then the MTT solution was removed and the formazan crystals were dissolved into 150 μL DMSO. The absorbance at 570 nm was showed on a microplate reader (Tecan, Austria). The percentage of cell viability was calculated as follows:

Cell viability % = (model-blank) / (control-blank) × 100%

4.6.2. Evaluation of MDCK cell monolayers

The formation of functional epithelial layers was monitored by measuring the transepithelial electrical resistance (TEER) with an epithelial volt-ohm meter in order to evaluate the integrity of the MDCK cell monolayers before each experiment [39]. Only cell monolayers with a TEER of above 200 Ω/cm^2 were used for the transport assays. The TEER values were also measured after the experiment to check monolayer integrity.

4.6.3. Preparation of transport samples

MDCK cells were seeded at the density of 5 × 10^4 cells/well on Transwell. Culture medium was replaced with fresh medium every two days, and the monolayers were grown for 4–5 days to reach confluence and differentiation after seeding. Before the experiments, the MDCK cell monolayers were washed three times with pre-warmed HBSS medium (pH 7.4), the monolayers were incubated in HBSS for 30 min at the finality. Then the drug solutions were added to either the apical (AP, 0.5 mL) or basolateral side (BL, 1.5 mL). 500 μL of the sample was collected from the opposite side at 150 min and then immediately frozen, lyophilized and preserved below −20 °C. Before quantitative analysis, the samples were dissolved in 100 μL water.

The apparent permeability coefficients (P_{app}) were calculated as:

P_{app}=dQ/dt × (1/C_0A)

P_{app}: apparent permeability coefficient (cm/s), dQ/dt: permeability rate of the compound on the receiver.

4.7. Chemistry methods

Common reagents and materials were purchased from commercial sources and used as received without further purification unless otherwise stated. Anhydrous ethanol (EtOH) was refluxed with magnesium powder and distilled under nitrogen before use. Anhydrous methanol (MeOH) and dichloromethane (DCM) were freshly distilled from CaH_2. Anhydrous dioxane was freshly distilled from anhydrous $CaCl_2$ prior to use. TLC plates were visualized by exposure to ultra violet light (UV). High resolution mass spectrometer (HRMS) data were acquired in positive ion mode using a Thermo Fisher LTQ ORBITRAP XL with an electrospray ionization (ESI) source. Nuclear magnetic resonance (NMR) spectra were acquired on a Bruker AV-300 spectrometer (300 MHz ^{1}H, 75 MHz ^{13}C). Chemical shifts (δ) are expressed in ppm downfield from tetramethylsilane (TMS) using non-deuterated solvent present in the bulk deuterated solvent ($CDCl_3$: ^{1}H 7.26 ppm, ^{13}C 77.16 ppm; DMSO-d_6: ^{1}H 2.50 ppm, ^{13}C 39.52 ppm). Data are represented as follows: chemical shift, multiplicity (s = singlet, d = doublet, t = triplet, m = multiplet, br = broad), coupling constant in Hertz (Hz), and integration. Detailed procedures with synthetic rout were exhibited in Scheme 2.

4.7.1. Synthetic and ^{1}H and ^{13}C NMR and HRMS characterization of compound **1** [40]

N^1,N^4-bis(4-carbamimidoylphenyl)succinamide (**1**). To a solution of 4-aminobenzamidine dihydrochloride (2.08 g, 10 mmol) in pyridine (8 mL) and DMF (40 mL) was added succinyl dichloride (0.56 mL, 5 mmol). The resulting mixture was stirred at 150 °C for 2 h, and a large amount of grey solid was generated. Then the reaction mixture was cooled to room temperature and filtrated. The filter cake was washed with water (20 mL) and acetone (20 mL) and dried under high vacuum for 3 h to give the crude compound **1**, which was purified by flash column chromatography to afford **1** (1.70 g, 48%) as a white solid. M.p. 218.3–220.9 °C (lit [40]. >300 °C in a dihydrochloride salt). ^{1}H NMR (300 MHz, DMSO-d_6) δ = 7.71 (d, J = 8.7 Hz, 4H), 7.61 (d, J = 8.7 Hz, 4H), 4.65–2.99 (m, 8H) 2.69 (s, 4H) ppm; ^{13}C NMR (75 MHz, DMSO-d_6): δ = 171.1, 171.1, 162.6, 162.6, 141.2, 141.2, 130.2, 130.2, 130.2, 130.2, 127.6, 127.6, 118.5, 118.5, 118.5, 118.5, 31.6, 31.6 ppm; HRMS (ESI-Orbitrap) m/z: [M + H]$^+$ calcd for $C_{18}H_{21}N_6O_2^+$ 353.1721; found 353.1719.

4.7.2. Synthetic and ^{1}H and ^{13}C NMR and HRMS characterization of compound **2** [41]

N^1,N^5-bis(4-carbamimidoylphenyl)glutaramide (**2**). Following the procedure described above for the synthesis of compound **1**, bisbenzamidine **2** (1.84 g, 50%) was prepared from 4-aminobenzamidine dihydrochloride and glutaryl dichloride. M.p. 213.5–214.6 °C (lit [41]. >300 °C in a dihydrochloride salt). ^{1}H NMR (300 MHz, DMSO-d_6): δ = 7.72 (d, J = 8.6 Hz, 4H), 7.63 (d, J = 8.6 Hz, 4H), 2.41 (t, J = 7.1 Hz, 4H), 1.99–1.84 (m, 2H) ppm; ^{13}C NMR (75 MHz, DMSO-d_6): δ = 171.5, 171.5, 162.7, 162.7, 141.2, 141.2, 131.1, 131.1, 131.1, 131.1, 127.2, 127.2, 127.2, 127.2, 118.7, 118.7, 36.0, 36.0, 21.2 ppm; HRMS (ESI-Orbitrap) m/z: [M + H]$^+$ calcd for $C_{19}H_{23}N_6O_2^+$ 367.1877; found 367.1873.

4.7.3. Synthetic and ^{1}H and ^{13}C NMR and HRMS characterization of compound **3** [41]

N^1,N^6-bis(4-carbamimidoylphenyl)adipamide (**3**). Following the procedure described above for the synthesis of compound **1**, bisbenzamidine **3** (2.09 g, 55%) was prepared from 4-aminobenzamidine dihydrochloride and adipoyl dichloride. M.p. 211.4–212.9 °C (lit [41]. >300 °C in a dihydrochloride salt). ^{1}H NMR (300 MHz, DMSO-d_6): δ = 7.71 (d, J = 8.1 Hz, 4H), 7.63 (d, J = 8.1 Hz, 4H), 2.37 (s, 4H), 1.63 (s, 4H) ppm; ^{13}C NMR (75 MHz, DMSO-d_6): δ = 171.9, 171.9, 162.9, 162.9, 141.5, 141.5, 130.2, 130.2, 130.2, 130.2, 127.8, 127.8, 118.6, 118.6, 118.6, 118.6, 36.7, 36.7, 25.2, 25.2 ppm; HRMS (ESI-Orbitrap) m/z: [M + H]$^+$ calcd for $C_{20}H_{25}N_6O_2^+$ 381.2034; found 381.2032.

4.7.4. Synthetic and ^{1}H and ^{13}C NMR and HRMS characterization of compound **4** [42]

N,N'-(propane-1,3-diyl)bis(4-cyanobenzamide) (**9**)**.** To a solution of propane-1,3-diamine (0.83 mL, 10 mmol) in Et_3N (2.8 mL) and DCM (30 mL) was added dropwise 4-cyanobenzoyl chloride (3.31 g, 20 mmol) in DCM at 0 °C by a constant pressure titration funnel, then warmed to ambient temperature. After stirring for 24 h, the solvent was removed under vacuum and the residue was washed with saturated aqueous $NaHCO_3$ (30 mL), hydrochloride acid aqueous (30 mL, 1 N) and water (30 mL) to give crude compound **9** (3.20 g). The crude product was recrystallized by (50–90)% aqueous DMSO to yield compound **9** (2.96 g, 89%) as a white solid. M.p. 215.2–216.1 °C (lit [42]. 212.5–213.5 °C). ^{1}H NMR (300 MHz, DMSO-d_6): δ = 8.77 (t, J = 5.4 Hz, 2H), 8.03–7.91 (m, 8H), 3.35 (dd, J = 12.7, 6.6 Hz, 4H), 1.81 (p, J = 6.9 Hz, 2H) ppm. ^{13}C NMR (75 MHz,

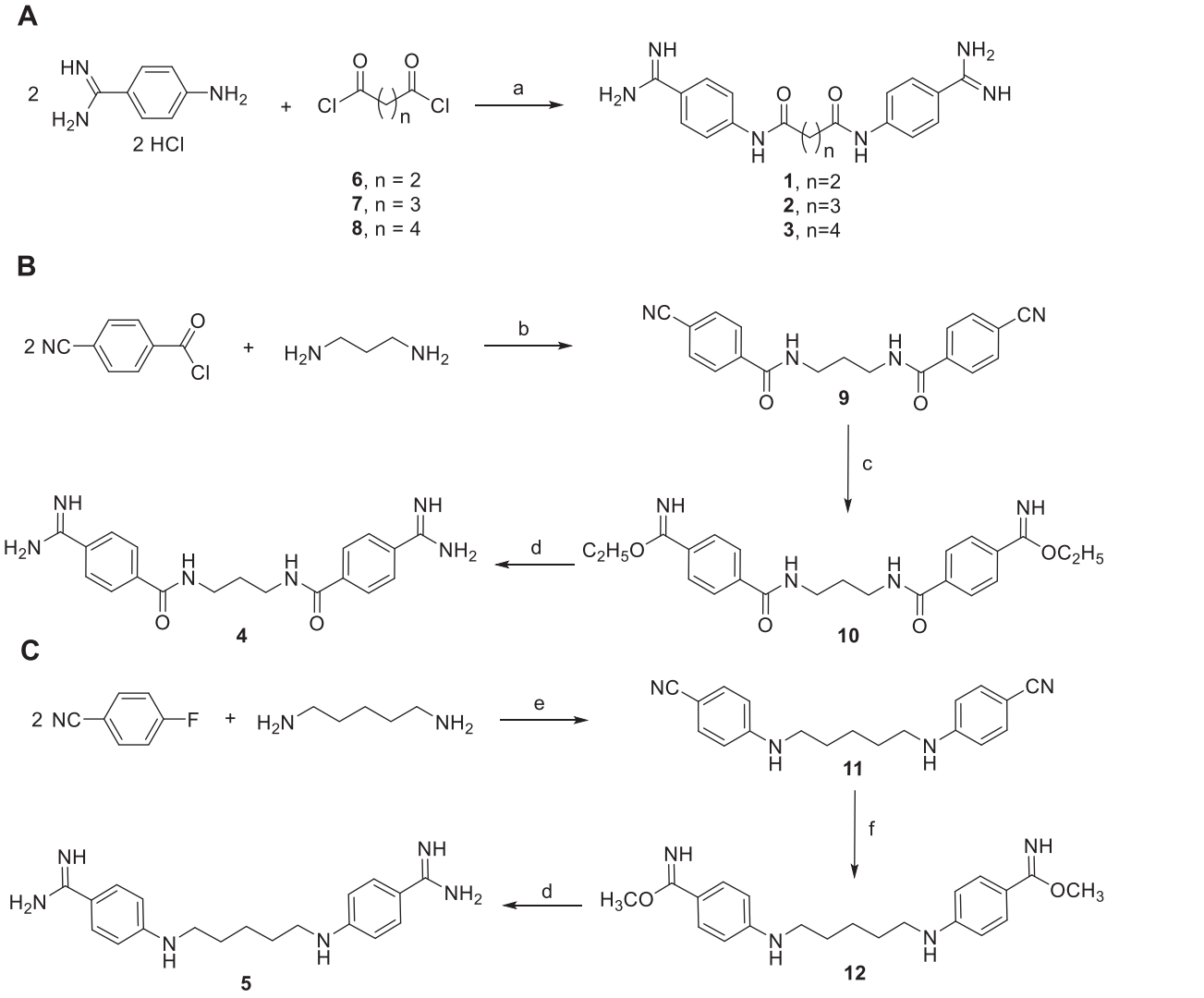

Scheme 2. Synthetic route for pentamidine analogues. Reagents and conditions: (a) pyridine, DMF, 150 °C; (b) DCM, Et_3N, ambient temperature; (c) EtOH, HCl (*gas*); (d) EtOH, NH_3 (*gas*), ambient temperature; (e) DMSO, Et_3N, 150 °C; (f) dioxane, MeOH, HCl (*gas*), ambient temperature.

DMSO-d_6): δ = 165.3, 165.3, 139.0, 139.0, 132.9, 132.9, 132.9, 132.9, 128.4, 128.4, 128.4, 128.4, 118.8, 118.8, 114.0, 114.0, 37.8, 37.8, 29.3 ppm; HRMS (ESI-Orbitrap) *m/z*: $[M + H]^+$ calcd for $C_{19}H_{17}N_4O_2^+$ 322.1273; found 322.1277.

Diethyl-4,4'-((propane-1,3-diylbis(azanediyl))bis(carbonyl)) dibenzimidate (**10**). To a solution of dry EtOH (50 mL) was bubbled fresh prepared HCl (gas) for 8 h under ice bath. Then compound **9** (2.0 g, 6.02 mmol) was added to the fresh ethanol solution of HCl (50 mL) and the reaction mixture was slowly warmed to ambient temperature. After vigorously stirred for 4 d, the reaction mixture was cooled in a freezer to form precipitate. The precipitate was filtered and the filter cake was washed with diethyl ether (3 × 100 mL), dried under high vacuum to yield crude compound **10** (1.76 g), which was unstable and used for the next step without further characterization and purification.

N,N'-(propane-1,3-diyl)bis(4-carbamimidoylbenzamide) (**4**). To a solution of dry EtOH (50 mL) was bubbled fresh prepared NH_3 (gas) for 8 h under ice bath. The compound **10** (1.76 g) was added to the saturated ethanolic ammonia solution (50 mL). The reaction mixture was sealed and slowly warmed to ambient temperature and vigorously stirred for 4 d. Then, the mixture was cooled in a freezer to form precipitate, which was filtrated, washed with water (10 mL) and dried under high vacuum to give compound **4** (0.90 g, 41% from compound **10**) as a white solid. M.p. 230.4–231.6 °C (lit [42]. 302.5–304.5 °C in a dihydrochloride salt). ^{1}H NMR (300 MHz, DMSO-d_6): δ = 8.59 (s, 2H), 7.85 (s, 8H), 6.48 (s, 6H), 3.34 (d, *J* = 5.2 Hz, 4H), 1.77 (m, 2H) ppm; ^{13}C NMR (75 MHz, DMSO-d_6): δ = 166.2, 166.2, 162.3, 162.3, 139.0, 139.0, 137.3, 137.3, 136.9, 136.9, 136.9, 136.9, 136.0, 136.0, 136.0, 136.0, 37.6, 37.6, 29.7, 29.7 ppm. HRMS (ESI-Orbitrap) *m/z*: $[M + H]^+$ calcd for $C_{19}H_{23}N_6O_2^+$ 367.1877; found 367.1875.

*4.7.5. Synthetic and ^{1}H and ^{13}C NMR and HRMS characterization of compound **5** [43]*

4,4'-(pentane-1,5-diylbis(azanediyl))dibenzonitrile (**11**) [44]. To a solution of 4-fluorobenzonitrile (11 g, 90 mmol) in Et_3N (14 mL) and DMSO (60 mL) was added pentane-1,5-diamine (2.3 g, 23 mmol). The reaction mixture was stirred at 150 °C for 3 h. Then the reaction mixture was poured into ice-water mixture (400 mL) and a large amount of pale-yellow solid was generated. The solid was filtered and recrystallized with DMSO/H_2O (8:1) to yield a pale yellow solid (5.3 g, 75%). M.p. 141.1–142.7 °C. ^{1}H NMR (300 MHz,

DMSO-d_6): δ = 7.42 (d, J = 8.7 Hz, 4H), 6.68 (t, J = 5.1 Hz, 2H), 6.60 (d, J = 8.8 Hz, 4H), 3.04 (dd, J = 12.2, 6.4 Hz, 4H), 1.56 (dt, J = 13.7, 7.0 Hz, 4H), 1.42 (dd, J = 14.3, 7.8 Hz, 2H) ppm. ^{13}C NMR (75 MHz, DMSO-d_6): δ = 152.7, 152.7, 133.8, 133.8, 133.8, 133.8, 121.2, 121.2, 112.1, 112.1, 112.1, 112.1, 95.7, 95.7, 42.5, 42.5, 28.6, 28.6, 24.6 ppm. HRMS (ESI-Orbitrap) m/z: $[M + H]^+$ calcd for $C_{19}H_{21}N_4^+$ 304.3970; found 304.3975.

Dimethyl-4,4'-(pentane-1,5-diylbis(azanediyl))dibenzimidate-dihydrochloride (**12**). To a solution of dry dioxane (50 mL) and dry MeOH (20 mL) was bubbled fresh prepared HCl (gas) for 8 h at ice bath. Then compound **11** (5.3 g) was added to the prepared solution (50 mL) and slowly warmed to ambient temperature and stirred for 1 h, then another portion of mixed solution (20 mL) was added to reaction. After stirring for 2 d, a large amount of precipitate was generated. The reaction mixture was filtered and the filter cake was washed with diethyl ether (100 mL), dried under reduced pressure to achieve crude compound **12** (4.7 g), which was unstable and used for the next step without further characterization and purification.

4,4'-(pentane-1,5-diylbis(azanediyl))dibenzimidamide (**5**). To a solution of dry EtOH (30 mL) was bubbled fresh prepared NH_3 (gas) for 8 h at −20 °C. Then compound **12** (1.0 g) was added to the saturated ethanolic ammonia solution (30 mL). The reaction mixture was sealed and slowly warmed to ambient temperature. After vigorously stirred for 3 d, a large amount of white solid was generated. The reaction mixture was filtered and the filter cake was dispersed to a solution of NaOH aqueous (30 mL, 1 M). After stirring for 40 min, the solid was filtered and the filter cake was washed with water (10 mL) and then dried under high vacuum to yield compound **5** (0.63 g, 23% from compound **11**) as a white solid. M.p. 161.6−163.2 °C (lit [45]. 215 °C in a tetrahydrochloride salt). ^{1}H NMR (300 MHz, DMSO-d_6): δ = 7.52 (d, J = 8.4 Hz, 4H), 6.51 (d, J = 8.5 Hz, 4H), 6.20 (s, br, 4H), 5.98 (m, 2H), 3.03 (m, 4H), 1.57 (m, 4H), 1.45 (m, 2H) ppm; ^{13}C NMR (75 MHz, DMSO-d_6): δ = 163.0, 163.0, 150.9, 150.9, 128.1, 128.1, 128.1, 128.1, 122.9, 122.9, 111.1, 111.1, 111.1, 111.1, 43.0, 43.0, 28.9, 28.9, 24.8 ppm; HRMS (ESI-Orbitrap) m/z: $[M + H]^+$ calcd for $C_{19}H_{27}N_6^+$ 339.2292; found 339.2294.

Declaration of competing interest

The authors declare that they have no known competing financial interests or personal relationships that could have appeared to influence the work reported in this paper.

Acknowledgements

This work was supported by the National Natural Science Foundation of China [21602216, 21877106, 21807098]; Chinese Academy of Sciences (CAS) Pioneer Hundred Talents Program; the Young Talents Program of Chinese Academy of Agricultural Sciences; and the Royal Society-Newton Advanced Fellowship (NA170152). Computing time was supported by the Network and Computing Center, Changchun Institute of Applied Chemistry, CAS, the China Science and Technology Cloud, the National Supercomputing Center in Shenzhen and the Beijing Super Cloud Computing Center (BSCC).

Appendix. Supplementary data

Supplementary data associated with this article can be found in the online version, at https://doi.org/10.1016/j.ejmech.2021.113210. These data include MOL files and InChiKeys of the most important compounds described in this article.

References

[1] V. Azzarito, K. Long, N.S. Murphy, A.J. Wilson, Inhibition of alpha-helix-mediated protein-protein interactions using designed molecules, Nat. Chem. 5 (2013) 161−173, https://doi.org/10.1038/Nchem.1568.
[2] M.P. Stumpf, T. Thorne, E. de Silva, R. Stewart, H.J. An, M. Lappe, C. Wiuf, Estimating the size of the human interactome, Proc. Natl. Acad. Sci. U. S. A. 105 (2008) 6959−6964, https://doi.org/10.1073/pnas.0708078105.
[3] S. Surade, T.L. Blundell, Structural biology and drug discovery of difficult targets: the limits of ligandability, Chem. Biol. 19 (2012) 42−50, https://doi.org/10.1016/j.chembiol.2011.12.013.
[4] T.A. Stone, C.M. Deber, Therapeutic design of peptide modulators of protein-protein interactions in membranes, Biochim. Biophys. Acta. Biomembr. 1859 (2017) 577−585, https://doi.org/10.1016/j.bbamem.2016.08.013.
[5] G.A. Caputo, E. London, Cumulative effects of amino acid substitutions and hydrophobic mismatch upon the transmembrane stability and conformation of hydrophobic alpha-helices, Biochemistry-US. 42 (2003) 3275−3285, https://doi.org/10.1021/bi026697d.
[6] N.J. Gleason, V.V. Vostrikov, D.V. Greathouse, R.E. Koeppe, Buried lysine, but not arginine, titrates and alters transmembrane helix tilt, Proc. Natl. Acad. Sci. U. S. A. 110 (2013) 1692−1695, https://doi.org/10.1073/pnas.1215400110.
[7] V.V. Vostrikov, B.A. Hall, D.V. Greathouse, R.E. Koeppe II, M.S. Sansom, Changes in transmembrane helix alignment by arginine residues revealed by solid-state NMR experiments and coarse-grained MD simulations, J. Am. Chem. Soc. 132 (2010) 5803−5811, https://doi.org/10.1021/ja100598e.
[8] G.A. Caputo, E. London, Position and ionization state of Asp in the core of membrane-inserted alpha helices control both the equilibrium between transmembrane and nontransmembrane helix topography and transmembrane helix positioning, Biochemistry-US. 43 (2004) 8794−8806, https://doi.org/10.1021/bi049696p.
[9] D.W. Sammond, C. Joce, R. Takeshita, S.E. McQuate, N. Ghosh, J.M. Martin, H. Yin, Transmembrane peptides used to investigate the homo-oligomeric interface and binding hotspot of latent membrane protein 1, Biopolymers 95 (2011) 772−784, https://doi.org/10.1002/bip.21672.
[10] B. Sugden, An intricate route to immortality, Cell. 57 (1989) 5−7, https://doi.org/10.1016/0092-8674(89)90165-7.
[11] D. Wang, D. Liebowitz, E. Kieff, An EBV membrane protein expressed in immortalized lymphocytes transforms established rodent cells, Cell. 43 (1985) 831−840, https://doi.org/10.1016/0092-8674(85)90256-9.
[12] K.M. Kaye, K.M. Izumi, E. Kieff, Epstein-barr-virus latent membrane protein-1 is essential for B-lymphocyte growth transformation, Proc. Natl. Acad. Sci. U. S. A. 90 (1993) 9150−9154, https://doi.org/10.1073/pnas.90.19.9150.
[13] U. Dirmeier, B. Neuhierl, E. Kilger, G. Reisbach, M.L. Sandberg, W. Hammerschmidt, Latent membrane protein 1 is critical for efficient growth transformation of human B cells by Epstein-Barr virus, Cancer. Res. 63 (2003) 2982−2989.
[14] J.I. Cohen, Epstein-Barr virus infection, N. Engl. J. Med. 343 (2000) 481−492, https://doi.org/10.1056/NEJM200008173430707.
[15] K.J. Flavell, P.G. Murray, Hodgkin's disease and the Epstein-Barr virus, Mol. Pathol. 53 (2000) 262−269, https://doi.org/10.1136/mp.53.5.262.
[16] G. Henle, W. Henle, V. Diehl, Relation of Burkitt's tumor-associated herpes-ytpe virus to infectious mononucleosis, Proc. Natl. Acad. Sci. U. S. A. 59 (1968) 94−101, https://doi.org/10.1073/pnas.59.1.94.
[17] G. Brady, G.J. MacArthur, P.J. Farrell, Epstein-Barr virus and Burkitt lymphoma, J. Clin. Pathol. 60 (2007) 1397−1402, https://doi.org/10.1136/jcp.2007.047977.
[18] A. Kieser, K.R. Sterz, The latent membrane protein 1 (LMP1), Curr. Top. Microbiol. Immunol. 391 (2015) 119−149, https://doi.org/10.1007/978-3-319-22834-1_4.
[19] E.F. Kot, Y. Wang, S.A. Goncharuk, B. Zhang, A.S. Arseniev, X. Wang, K.S. Mineev, Oligomerization analysis as a tool to elucidate the mechanism of EBV latent membrane protein 1 inhibition by pentamidine, Biochim. Biophys. Acta. Biomembr. 1862 (2020), 183380, https://doi.org/10.1016/j.bbamem.2020.183380.
[20] X. Wang, J.P. Saludes, T.X. Zhao, A. Csakai, Z. Fiorini, S.A. Chavez, J. Li, G.I. Lee, K. Varga, H. Yin, Targeting the lateral interactions of transmembrane domain 5 of Epstein-Barr virus latent membrane protein 1, Biochim. Biophys. Acta. Biomembr. 1818 (2012) 2282−2289, https://doi.org/10.1016/j.bbamem.2012.05.013.
[21] X. Wang, Z. Fiorini, C. Smith, Y. Zhang, J. Li, L.R. Watkins, H. Yin, Repositioning antimicrobial agent pentamidine as a disruptor of the lateral interactions of transmembrane domain 5 of EBV latent membrane protein 1, PloS. One. 7 (2012), e47703, https://doi.org/10.1371/journal.pone.0047703.
[22] Y. Wang, Y. Peng, B. Zhang, X. Zhang, H. Li, A.J. Wilson, K.S. Mineev, X. Wang, Targeting trimeric transmembrane domain 5 of oncogenic latent membrane protein 1 using a computationally designed peptide, Chem. Sci. 10 (2019) 7584−7590, https://doi.org/10.1039/c9sc02474c.
[23] E. Lindner, D. Langosch, A ToxR-based dominant-negative system to investigate heterotypic transmembrane domain interactions, Proteins. 65 (2006) 803−807, https://doi.org/10.1002/prot.21226.
[24] W.P. Russ, D.M. Engelman, TOXCAT: a measure of transmembrane helix association in a biological membrane, Proc. Natl. Acad. Sci. U. S. A. 96 (1999) 863−868, https://doi.org/10.1073/pnas.96.3.863.
[25] Schrödinger Release 2015-2: Maestro, Schrödinger, LLC, New York, NY, 2015.

[26] O. Trott, A.J. Olson, Software news and update AutoDock Vina: improving the speed and accuracy of docking with a new scoring function, efficient optimization, and multithreading, J. Comput. Chem. 31 (2010) 455–461, https://doi.org/10.1002/jcc.21334.
[27] S. Jo, T. Kim, V.G. Iyer, W. Im, CHARMM-GUI: a web-based graphical user interface for CHARMM, J. Comput. Chem. 29 (2008) 1859–1865, https://doi.org/10.1002/jcc.20945.
[28] R.B. Best, X. Zhu, J. Shim, P.E. Lopes, J. Mittal, M. Feig, A.D. Mackerell Jr., Optimization of the additive CHARMM all-atom protein force field targeting improved sampling of the backbone phi, psi and side-chain chi(1) and chi(2) dihedral angles, J. Chem. Theory. Comput. 8 (2012) 3257–3273, https://doi.org/10.1021/ct300400x.
[29] J.B. Klauda, R.M. Venable, J.A. Freites, J.W. O'Connor, D.J. Tobias, C. Mondragon-Ramirez, I. Vorobyov, A.D. MacKerell Jr., R.W. Pastor, Update of the CHARMM all-atom additive force field for lipids: validation on six lipid types, J. Phys. Chem. B. 114 (2010) 7830–7843, https://doi.org/10.1021/jp101759q.
[30] K. Vanommeslaeghe, E. Hatcher, C. Acharya, S. Kundu, S. Zhong, J. Shim, E. Darian, O. Guvench, P. Lopes, I. Vorobyov, A.D. Mackerell Jr., CHARMM general force field: a force field for drug-like molecules compatible with the CHARMM all-atom additive biological force fields, J. Comput. Chem. 31 (2010) 671–690, https://doi.org/10.1002/jcc.21367.
[31] L. Huang, B. Roux, Automated force field parameterization for nonpolarizable and polarizable atomic models based on ab initio target data, J. Chem. Theory. Comput. 9 (2013) 3543–3556, https://doi.org/10.1021/ct4003477.
[32] J.C. Phillips, R. Braun, W. Wang, J. Gumbart, E. Tajkhorshid, E. Villa, C. Chipot, R.D. Skeel, L. Kale, K. Schulten, Scalable molecular dynamics with NAMD, J. Comput. Chem. 26 (2005) 1781–1802, https://doi.org/10.1002/jcc.20289.
[33] G.J. Martyna, D.J. Tobias, M.L. Klein, Constant-pressure molecular-dynamics algorithms, J. Chem. Phys. 101 (1994) 4177–4189, https://doi.org/10.1063/1.467468.
[34] S.E. Feller, Y.H. Zhang, R.W. Pastor, B.R. Brooks, Constant-pressure molecular-dynamics simulation - the Langevin piston method, J. Chem. Phys. 103 (1995) 4613–4621, https://doi.org/10.1063/1.470648.
[35] U. Essmann, L. Perera, M.L. Berkowitz, T. Darden, H. Lee, L.G. Pedersen, A smooth particle mesh Ewald method, J. Chem. Phys. 103 (1995) 8577–8593, https://doi.org/10.1063/1.470117.
[36] S. Kumar, D. Bouzida, R.H. Swendsen, P.A. Kollman, J.M. Rosenberg, The weighted histogram analysis method for free-energy calculations on biomolecules. I. The method, J. Comput. Chem. 13 (1992) 1011–1021, https://doi.org/10.1002/jcc.540130812.
[37] A. Grossfield, WHAM: the weighted histogram analysis method", version 2.0.9. http://membrane.urmc.rochester.edu/wordpress/?page_id=126.
[38] Y. Wang, R.K. Finol-Urdaneta, V.A. Ngo, R.J. French, S.Y. Noskov, Bases of bacterial sodium channel selectivity among organic cations, Sci. Rep. 9 (2019), 15260, https://doi.org/10.1038/s41598-019-51605-y.
[39] F. Ingels, B. Beck, M. Oth, P. Augustijns, Effect of simulated intestinal fluid on drug permeability estimation across Caco-2 monolayers, Int. J. Pharm. 274 (2004) 221–232, https://doi.org/10.1016/j.ijpharm.2004.01.014.
[40] J.J. Vanden Eynde, A. Mayence, M. Mottamal, C.J. Bacchi, N. Yarlett, M. Kaiser, R. Brun, T.L. Huang, Alkanediamide-Linked bisbenzamidines are promising antiparasitic agents, Pharmaceuticals (Basel). 9 (2016), https://doi.org/10.3390/ph9020020.
[41] T.L. Huang, J.J. Vanden Eynde, A. Mayence, M.S. Collins, M.T. Cushion, D. Rattendi, I. Londono, L. Mazumder, C.J. Bacchi, N. Yarlett, Synthesis and SAR of alkanediamide-linked bisbenzamidines with anti-trypanosomal and anti-pneumocystis activity, Bioorg. Med. Chem. Lett. 19 (2009) 5884–5886, https://doi.org/10.1016/j.bmcl.2009.08.073.
[42] D. Maciejewska, J. Zabinski, P. Kazmierczak, M. Rezler, B. Krassowska-Swiebocka, M.S. Collins, M.T. Cushion, Analogs of pentamidine as potential anti-Pneumocystis chemotherapeutics, Eur. J. Med. Chem. 48 (2012) 164–173, https://doi.org/10.1016/j.ejmech.2011.12.010.
[43] J.N. Ashley, H.J. Barber, A.J. Ewins, G. Newbery, A.D.H. Self, A chemotherapeutic comparison of the trypanocidal action of some aromatic diamidines, J. Chem. Soc. (1942) 103–116, https://doi.org/10.1039/jr9420000103.
[44] R.R. Tidwell, S.K. Jones, J.D. Geratz, K.A. Ohemeng, M. Cory, J.E. Hall, Analogs of 1,5-bis(4-Amidinophenoxy)Pentane (pentamidine) in the treatment of experimental pneumocystis-carinii pneumonia, J. Med. Chem. 33 (1990) 1252–1257, https://doi.org/10.1021/jm00166a026.
[45] S.M. Bakunova, S.A. Bakunov, D.A. Patrick, E.V.K.S. Kumar, K.A. Ohemeng, A.S. Bridges, T. Wenzler, T. Barszcz, S.K. Jones, K.A. Werbovetz, R. Brun, R.R. Tidwell, Structure-activity study of pentamidine analogues as anti-protozoal agents, J. Med. Chem. 52 (2009) 2016–2035, https://doi.org/10.1021/jm801547t.